Ionospheric density oscillations associated with recurrent prompt penetration electric fields during the space weather event of 04 November 2021 over the East-Asian sector

Ram Singh[1], Y.S Lee[1], S.M. Song[1], Y.H. Kim[1], J.-Y. Yun[2], S. Sripathi[3], B. Rajesh[3]

[1]Department of Astronomy and Space Science, Chungnam National University, Daejeon, South Korea

[2]Forecast &Observation Division, Korea Space Weather Center (KSWC), Jeju, South Korea

[3]Indian Institute of Geomagnetism (IIG), Mumbai, India

Corresponding author: Young-Sook Lee (yslee0923@cnu.ac.kr)

Abstract

We found the signatures of the multiple prompt penetration electric fields (PPEF) and the disturbance dynamo (DD) electric field having impacts on the East Asian sector ionosphere along the meridional chain thoroughly from the equator, low-mid to high latitudes during the space weather event of 03-05 November 2021. The observation is made on GPS-TEC, digisonde, and magnetometer stations. In the main phase of the storm, intense modulations of VTEC (vertical total electron content) and foF2 (critical frequency) are observed as coherently fluctuating with IEF (interplanetary electric field) and IMF Bz reorientations. It is diagnosed that the oscillations in the DP2 (disturbance polar current 2) current system directly penetrate meridianally from high to equatorial latitudes, leading to the significant changes in ionospheric electrodynamics that governs the density fluctuations. The wavelet spectra of VTEC, foF2, h'F (virtual height), H-components and IEF give a result of common and dominant periodicity occurring at ~1hr. This result suggests that the wavelike oscillations of VTEC and foF2 and H component are associated with PP electric fields.

Plain Language Summary:

Geomagnetic storm time electrodynamics of the ionosphere is severely affected by magnetospheric convection electric field induced by solar wind-induced magnetospheric dynamo, and ionospheric disturbance dynamo (DD) generated by global thermospheric wind

circulation and joule heating at high latitude. The Magnetospheric convection electric field can penetrate instantly into the equatorial ionosphere known as prompt penetration (PP) electric field, while, the thermospheric wind and its associated disturbances can reach at the equator with a time delay. During the main phase of the storm, observations showed intense modulations in vertical total electron content (VTEC), critical frequency (foF2) from equator to high latitudes associated with PP electric fields. In recovery phase, disturbances in VTEC, foF2, and virtual height (h'F) are caused by either DD electric field or traveling ionospheric disturbances (TIDs). Further analysis in this study suggests the evidence of causal relationship among the interplanetary electric field, DP2 current system, and ionospheric density oscillations. Wavelets analysis shows a common and dominant periodicity of ~1 hr in interplanetary and ionospheric parameters.

Keywords: Ionospheric electrodynamics; high-mid-low latitude ionosphere; geomagnetic storm, GPS-TEC, prompt penetration of electric field (PPEF), digisonde

Key Results:

(1) PPEF signature observed along the ionosphere meridian in East-Asia.
(2) Infiltration of DP2 current to the equator to cause the ionospheric density fluctuations.
(3) The oscillations of the observed parameters (TEC, foF2, and H-component) along the meridional chain coincide with that of IEF at a ~1hr periodicity.

1. Introduction

It is well known that the interplanetary and geomagnetic conditions play a significant role in the interaction between the magnetosphere and ionosphere during geomagnetic storms. The high-speed solar wind interacts with the magnetosphere and discharges its energy into the high latitude ionosphere through magnetospheric field-aligned currents (FACs) and other sources (Araki et al., 1985; Nishida, 1968b; Spiro et al., 1988; Kikuchi et al., 1996, 2008). This energy blows towards the equator in the form of neutral winds, electric fields, or other processes, that can modify the electrodynamics of the ionosphere (Blanc and Richmond, 1980; Sastri et al., 2000; Abdu et al., 1998). The modifications in the electrodynamics of the magnetosphere-ionosphere system can impact space and ground-based technological systems. The main phase of a geomagnetic storm, which is associated with ring current intensification, leads to large changes in the electrodynamics of equatorial and low latitude ionospheres, playing as a risk

factor for power systems at middle and low latitudes (Gaunt and Coetzee, 2007; Liu et al., 2009).

At the equatorial and low latitudes the ionospheric electric field and currents are mainly driven by the prompt penetration electric field (PPEF) induced by the magnetospheric convection electric field associated with the solar-wind magnetosphere dynamo (Araki et al., 1985; Kikuchi et al.,1996, 2008; Spiro et al., 1988). Neutral wind perturbations caused by storm-induced high-latitude joule heating can change thermospheric general circulation and plasma dynamics. Ions can move either along or perpendicular to the magnetic field by the ion neutral collision caused by the neutral wind disturbance. Parallel ion drift can generate the traveling ionospheric disturbance (TID), and perpendicular ion drift is associated with zonal electric field established by disturbance wind dynamo to be induced during the equatorward propagation of disturbance winds. Therefore, the lower latitude ionospheres are significantly affected either by the ionospheric disturbance dynamo electric field (DDEF) or TID (Fujiwara et al., 1996; Blanc and Richmond, 1980; Abdu et al., 2007). For the PPEF the ionospheric convection electric field, which is projected from the magnetosphere, promptly induce DP2 current (disturbance polar current 2) system in the dusk and dawn sides at the equatorward edges in the convection zones, and then the effects of DP2 currents promptly penetrate into the low and equatorial latitudes.

The effects of PP electric field instantaneously penetrate into the equator by the propagation of eastward/westward polarity in the transverse magnetic mode (TM0) through the Earth Ionosphere waveguide in the dayside/nightside (Kikuchi et al., 1996; 2008). However, the DD electric field reaches at the equator with a delay depending upon its propagation speed with westward/eastward polarity on the dayside/nightside. The DD electric field disturbances are long-lasting, and their impacts on the equatorial and low-latitude ionosphere can be seen up to about a day or two after the onset of a geomagnetic storm (Blanc and Richmond, 1980; Sastri et al., 2000; Abdu et al., 2007).

The storm time ionospheric electric field perturbations affect the distribution of ionospheric plasma density by generating positive and negative ionospheric storms. It is known that the enhancement in electron density/total electron content (TEC)/maximum frequency of F2 peak (foF2) as compared to quiet time variation is considered as positive ionospheric storm, while the reduction of electron density/TEC/foF2 is termed with the negative ionospheric storm. The

positive ionospheric storms can be generated by plasma redistribution due to disturbed electric fields (Balan et al., 2010; Ram Singh et al., 2015; Fagundes et al., 2016; Sreedevi and Choudhary., 2017), by thermospheric winds (Rishbeth, 1975; Prolss, 1993; Lin et al., 2005), by composition changes and an increase in the oxygen density (Rishbeth, 1998; Fuller-Rowell et al., 1996), or by traveling ionospheric disturbances (TIDs) (Prolss., 1978; Goncharenko et al., 2007). However, the negative ionospheric storms are attributed to an increase of molecular nitrogen density relative to atomic oxygen (Prolss et al., 1988; Rishbeth, 1998). Several authors investigated positive and negative ionospheric storm effects on the topside and bottom side ionospheres using the GPS-TEC and ground based ionosondes (Zhao et al., 2012; Fagundes et al., 2016; Lima et al., 2004; Kelley et al., 2004; Ram Singh and Sripathi., 2017). Fagundes et al. (2016) reported positive ionospheric storms in F-region density distribution, which were associated with the strong eastward PPEF over the Brazilian sector during the main phase of the magnetic storm on 17 March 2015. Kelley et al. (2004) suggested that the daytime eastward PPEF can generate negative storms in Nmax (maximum electron density) and TEC at the equatorial latitudes, while positive storms at the higher latitudes may occur through the enhanced plasma by fountain effects (Balan et al., 2010). Several modeling studies also suggested that the PPEF alone can produce positive ionospheric storms (Lin et al., 2005; Joshi et al., 2016).

The turning of the interplanetary magnetic field Bz plays an important role in characterizing the dawn to dusk convection electric field ($Ey = -Vx \times Bz$) in the magnetosphere, which penetrates into the polar ionosphere and finally generates the DP1 (disturbance polar current 1) and DP2 current systems in the high-latitude ionosphere (Nishida, 1968b; Araki et al., 1985; Kikuchi et al., 1996). The DP1 and DP2 current systems are originated from auroral electrojets and magnetic perturbations, which are generated by substorms and the convective system in the magnetosphere, respectively. When the polarity of IMF Bz suddenly turns from north to south, the magnetospheric convection electric field is intensified DP2 current system fluctuates and extends its effects down to the equatorial latitudes until the plasmasphere is electrically shielded (Nishida, 1968b). During the northward turning of IMF Bz, the intensity of the convection electric field is reduced and a strong electric field becomes effective in the plasmasphere that has the opposite polarity (dusk to dawn) (Kelley et al., 1979; Araki et al., 1985; Kikuchi et al., 1996). The DP2 current system is directly associated with the magnetospheric convection or the turning of IMF Bz. The impact can be detected at all latitudes

with different magnitudes (Clauer and Kamide, 1985). Using the spacecraft and ground magnetometer observations, many studies have suggested that the DP2 current disturbances are global, characterized by the quasi-periodic magnetic fluctuations with a timescale of 30 min to several hours (Nishida, 1968b; Kikuchi et al., 2008; Chakrabarty et al., 2008; Yizengaw et al., 2016; Rout et al., 2017; Huang., 2019a, 2020).

Several studies have focused on the fluctuations of DP2 currents and their impact on magnetic fluctuations in the equatorial ionosphere (Nishida, 1968b; Yizengaw et al., 2016; Huang., 2019a, 2020). Nishida (1968b) reported that the DP2 currents in the high-latitude and equatorial regions coherently fluctuate with IMF Bz, and the presence of DP2 current fluctuations at the equator are the direct result of quasi-periodic oscillations of IEF (interplanetary electric field) penetrating into the magnetosphere, and reaching down to the equatorial ionosphere (Kikuchi et al., 2008). The fluctuations of DP2 current systems in the high-latitude and the equatorial ionospheres are primarily driven by the fluctuations of IMF Bz (Yizengaw et al., 2016; Huang., 2019a, 2020). Yizengaw et al. (2016) presented coherent fluctuations of the IMF Bz, ionospheric DP2 currents, GPS TEC at the equatorial latitudes, and equatorial electrojet (EEJ). They suggested that the DP2 current fluctuations are generated by the reorientations of IMF Bz, which penetrate into the equatorial ionosphere and produce the fluctuations in the GPS TEC and EEJ.

Although DP2 current systems and their impact on magnetic fluctuations in the equatorial ionospheric region were studied in quite a few ways (Nishida, 1968b; Clauer and Kamide, 1985; Kikuchi et al., 1996, 2008), there are still several important questions remained unsolved. The main question is whether the impact of the DP2 current system can disturb the ionospheric density distribution at all latitudes at the same time. This study investigates the response of the ionospheric density distribution to the fluctuations of the DP2 current system at the high-mid and low latitudes over the East Asian sector during an intense geomagnetic storm on 03-05 November 2021.

This article is organized in the following manner: the data sources of the analysis are presented in section 2. In section 3, observations and results are presented. The space weather conditions and ground based observations are presented in sections 3.1 and 3.2. The cross-correlation analysis is present in section 3.3. In section 3.4, the wavelet analysis is performed to find a

common periodicity of VTEC, H-component, foF2, h'F, and IEFy. Discussions and conclusions are presented in sections 4 and 5, respectively.

2. Data Sets

To investigate the ionospheric response to the space weather event of 03-05 November 2021, we analyzed multi-instrument data sets over the East Asian sector. Solar wind parameters were obtained from the CDAWeb (http://cdaweb.gsfc.nasa.gov/). The 1 min time resolution solar wind data (in GSM coordinates) are measured by the ACE satellite, which is located near the L1 point. The vertical TEC (VTEC) data were obtained from a meridional chain of GPS receivers over the East Asian sector from (ftp://cddis.gsfc.nasa.gov/pub/gps/data, C. Noll, 2010), and 5 min interval GPS TEC data were collected from MIT Haystack Observatory Madrigal database (http://madrigal.haystack.mit.edu/madrigal/). The ionospheric parameters, namely, h'F (virtual height) and foF2 data were obtained from ionosondes operating at Guam (GUA: 13.69°N, 144.86°E, Geom. 6.12^{o}N), Sanya (SA: 18.53^{o}N, 109.61^{o}E, Geom. 8.87^{o}N), Wuhan (WU: 30.50^{o}N, 114.40^{o}E, Geom. 21.04^{o}N), Jeju (JJ: 33.43°N, 126.30°E, Geom. 24.36^{o}N), Icheon (ICN: 37.14°N, 127.54°E, Geom. 28.11^{o}N), Beijing (BP: 40.30^{o}N, 116.20^{o}E, Geom. 30.85^{o}N), and Mohe (MH: 52.00^{o}N, 122.52^{o}E, Geom. 42.73^{o}N). The ionograms at JJ, ICN, and BP are recorded in 15 min intervals, while the time interval of the ionograms at GUA, SA, WU, and MH is ~7 min. Ionosonde data were collected from Global Ionosphere Radio Observatory (GIRO) web (https://giro.uml.edu/didbase/). The geomagnetic activity indices of the symmetric component of ring current (SYM-H) and Kp index were obtained from the WDC (http://wdc.kugi.kyoto-u.ac.jp/). Magnetic field data were taken from the SuperMAG magnetometer network (http://supermag.jhuapl.edu) and the Korean space weather center (https://spaceweather.rra.go.kr). Details of the GPS TEC stations, ionosondes, and magnetometers with name, station code, latitudes, and longitudes are listed in Table 1, and the location of stations used in the present study are shown in Figure 1.

3. Observational Results

3.1 Space weather conditions during the storm of 03-05 November 2021

In this study, we report the unique observation of the quasi-periodic oscillations of the electron density at the high-mid and low latitude ionosphere over the East Asian sector caused by the PP electric field. Figure 2 shows interplanetary and geomagnetic conditions during an intense space weather event of 03-04 November 2021. Figure 2 shows, from the top, (a) variations of solar wind dynamic pressure (Pdyn, red), proton density (Np, black); (b) solar wind velocity (Vsw); (c) the y and z-components of interplanetary magnetic field (IMF), By (blue) and Bz (red); (d) the dawn-dusk component of interplanetary electric field (IEF), Ey, calculated from $Ey = (-Vx \times Bz)$; (e) the symmetric component of the ring current (Sym-H) demonstrating the evolution of magnetic storm; (f) the variation of equatorial electrojet (EEJ, blue) along with quiets days mean variation (black), EEJ calculated by subtracting the H-component from equatorial to off equatorial station ($EEJ = H_{GUA}\text{-}H_{KNY}$; LT = UT+9 hr); and (g) Kp indices, which describes the global geomagnetic disturbances. The vertically shaded region indicates the main phase of the storm, in which significant changes occurred in interplanetary and geomagnetic conditions. Sudden storm commencement (SSC) occurred at 20:30 UT on November 03, and Sym-H value reached its maximum of +45 nT at 21:00 UT. In addition, the corresponding sudden increased in Pdyn, Np, and Vsw were observed with reaching from ~1 to 20 nPa, ~1 to 20 cm^{-3}, and ~450 to 750 km s^{-1}, respectively. At the same time, IMF Bz turned southward direction and reached up to -15 nT. Since the main phase of the magnetic storm had started at 21:30 UT on November 3, Sym-H reached its minimum value of ~ -117 nT on November 4 at 12:00 UT. The recovery phase started after 12:00 UT on November 4, lasting for a few days. In the shaded region, IMF Bz shows bipolar fluctuations (from positive to negative and negative to positive) between $\sim \pm 15$ nT, and oscillation periods are between ~ 0.5 to 2 hours. Each negative (southward) and positive (northward) turning of the Bz correspond to an enhancement (duskward) and reduction (dawnward) of IEFy, respectively. During the main phase of the magnetic storm, the Kp value reached ~7.

3.2 GPS TEC and Ionosonde Observations

To study the TEC variations due to the present geomagnetic storm on November 4, 2021, ten GPS stations are selected over the East Asian sector between 110^o -150^o E longitudes, and a meridional chain of GPS receivers from high to equatorial latitudes. To compare any differences between geomagnetically quiet and disturbed days, Figures 3a-j show VTEC variations from the equator to high latitudes in the period of November 3-5, 2021. The VTEC during disturbed

period is presented in solid red color lines, the average VTEC value of five international quiet days (IQDs) (IQD's are the days where the geomagnetic variations are a minimum in each month) in black solid lines, and the standard deviation of five IQDs in gray bands. During November 2021, the five IQDs are 11, 12, 13, 14, and 26. The vertically shaded areas (blue) show multiple enhancements of VTEC compared to the mean on quiet days during the main phase of the storm. It is very useful to highlight the occurrence of positive and negative ionospheric storm effects by comparing VTEC between quiet and disturbed days. Here, the disturbed VTEC clearly demonstrates three strong positive ionospheric storms with the three peaks. In the disturbed period, the VTEC takes sudden enhancements and wavelike oscillations from equatorial to high latitude regions (from -6.67-71.63^{o} N GLat.), differentiated from the usual diurnal variation in a quiet condition. The first positive storm peak occurred at ~00:30 UT (09:30 LT) (up to ~ 43.79^{o}N GLat.), the second peak at ~04:30 UT (14:00 LT) (up to ~ 62.03^{o}N GLat.), and the third peak at ~09:30 UT (18:30 LT) (up to ~ 71.63^{o}N GLat.) as indicated with blue dashed vertical lines, and other multiple peaks are also observed in between with low strengths. The multiple peaks of VTEC occur almost at the same time with different strengths from the equator to high latitudes during the entire main phase of the storm from ~21:00 UT on 03rd to ~12:00 UT on 04th November. The almost simultaneous enhancements of VTEC occurring from the low to mid latitudes are attributed to the meridional effects of the PPEF, rather than to TID or any other sources. The VTEC variations at high latitude stations at TIXI and YAKT do not synchronize with those of lower latitude stations. At high latitudes, along with the PP electric field, other magnetospheric and ionospheric disturbances (e.g., particle precipitation, auroral heating, etc.) also may play a role in modifying the high latitude ionospheric electrodynamics. In the meanwhile, the enhancements/reductions (positive/negative storm) in VTEC were also observed in the recovery phase of the magnetic storm on 04-05th November. In Figure 3, it can be seen that between 12:00-15:00 UT (21:00-00:00 LT) on 04th November, increases in the VTEC were present from the equator to high latitudes. On 04-05 November around 22:00-02:00 UT (07:00-11:00 LT), the enhancements were observed from PIMO to CHAN, at the same time reduction in VTEC was observed at LAE. Thereafter, significant reductions in VTEC were observed at the low latitude stations at HKWS and LAE between 05:00 and 12:00 UT (14:00 and 21:00 LT) on November 5. The simultaneous occurrence of positive ionospheric storm at the mid-equatorial latitudes strongly implies the PP electric field-induced perturbations, while the sequential occurrence from mid-latitude first and then to low and equatorial latitudes

suggests the association with DD electric field or other sources (Lima et al., 2004; Abdu et al., 2007; Fagundes et al., 2016).

It is noticed from Figure 3 that the positive ionospheric storm peaks are not similar strengths at all latitudes. In Figure 4 the maps of (a) GPS TEC and (b) deviations of TEC (ΔTEC) are shown with universal time and geographical latitudes (-70~70^{o}N) for an East Asian Sector at ~130^{o} E $\pm$ 20^{o} longitudes on November 3-5, 2021. Here ΔTEC = (TEC- mean (TEC_{IQDs})) is the absolute difference of TEC from the five IQDs mean during the month of November. From Figure 4a, it is clearly noticed that the Equatorial Ionization Anomaly (EIA) is significantly enhanced, and two crests of EIA extend toward the higher latitudes during the main phase on November 4. In the recovery phase, EIA crests are significantly suppressed or absent for November 5. In Figure 4, at ~ 00:30 UT on Nov. 4, significant enhancement was observed from low to high latitudes (up to ~50^{o} N GLat). Another significant increase occurred from low to high latitudes (up to ~65^{o} N GLat) between ~03:00 and 07:00 UT, and between ~07:00 and 12:00 UT enhancements were observed in TEC up to mid latitudes. Figure 4b displays the significant multiple enhancements in terms of ΔTEC, as indicated by p1, p2, and p3 that occurred simultaneously from the equator to high latitudes (~70^{o} N GLat) in the northern hemisphere on November 4. The ΔTEC increase was more pronounced in the northern hemisphere than in the southern hemisphere. This hemispheric asymmetry in ΔTEC could be caused by the winter anomaly (or seasonal anomaly) effect. During the solstice, at low latitudes, the summer to winter hemispheric transequatorial neutral winds can transport the plasma from the summer to the winter hemisphere, causing higher plasma densities and a more amplified EIA crest in the winter hemisphere, known as the winter anomaly (Walker, 1981; Rishbeth, 2000). During the recovery phase on November 5, the ΔTEC shows reductions (negative ionospheric storm, indicated by n1 and n2) at low latitudes in the northern and southern hemispheres. In Figure 4, it may be noticed that the reduction in ΔTEC was more appeared in the southern hemisphere than in the northern hemisphere. The more appearance of the negative ionospheric storm in the southern hemisphere could be driven by the combined effects of disturbance electric fields and the winter anomaly effect.

To investigate the meridional features of the F-region over the East Asian sector a latitudinal chain of ionosondes is used. Figure 5 displays the variations of critical frequency of the F2 layer (foF2) from the equator to higher latitude stations at GUA, SA, WU, JJ, ICN, BP, and MH between 18:00 UT (03:00 LT) on November 3-23:59 UT (08:00 LT) on November 4. In

Figures 5a-g, the variations of foF2 during the storm days are plotted in red lines, and the mean value and standard deviation of quiet days at respective stations are overlapped in grey lines including error bars. In Figures 5a-g, it can be clearly seen the pronounced enhancements/reductions of foF2 are observed at all stations in the main phase between ~21:00 UT (06:00 LT) on November 3 and 12:00 UT (21:00 LT) on November 4. The vertical dashed black lines indicate the simultaneous enhancements of foF2 from the equator to higher latitude stations. However, in the recovery phase, foF2 shows density fluctuations with time delay from higher to lower latitudes as indicated by the blue color dashed line. The first peak in density was observed at high latitude station at MH ~12:30 UT (21:00 LT) and after ~2.5 hrs reached at equatorial station at GUA ~15:00 UT (00:00 LT). In the main phase, repeated enhancements of foF2 are typical for the events of PP electric fields, however, in the recovery phase density oscillations can be associated with DD electric field or TIDs (Lima et al., 2004; Abdu et al., 2007; Liu et al., 2014; Fagundes et al., 2016). The signature of DD electric field can be observed in h'F. In Figures 6a-f grey lines with error bars indicate the temporal variations of mean h'F at GUA, SA, WU, ICN, BP, and MH for quiet days. The vertically shaded region (grey) represents the main phase of the storm. During the main phase, h'Fs at all stations show normal behavior without reflecting a significant storm effect. In the meanwhile, at the equatorial station GUA height shows multiple oscillations with a large enhancement at 03:00 UT (12:00 LT) and 09:00 UT (18:00 LT). The reductions in h'F were observed during the weakening of the eastward electric field, as EEJ showed in Figure2f, at ~01:00 UT (10:00 LT), 05:00 UT (14:00 LT), and 10:00 UT (19:00 LT). In the recovery phase from ~12:00-21:00 UT (21:00-06:00 LT) multiple peaks of h'F with significant changes are observed with time delay. From the figure, the ionospheric height enhancements can be seen first at the high latitude station (MH) and after ~2.5 hrs delay such enhancement can be seen over the equatorial station (GUA), as shown with blue color dashed lines. Based on the peak occurrence of h'F and foF2, the propagation speed of disturbances was calculated to give a result of time delay (~2.5 hrs) for the distance between two stations of MH and GUA (~4300 km). The phase propagation speed of disturbance is ~477 m/s, which matches with the characteristics of TIDs (Lima et al., 2004; Lee et al., 2004). Generally, the horizontal wavelength of TIDs varies from 100-1000 km with the periods ranging from few minutes to hours and propagation speed ranged from 50-1000 m/s. During the magnetic storm time, TIDs may be generated due to a large amount of energy deposition and joule heating, and they can propagate towards the low latitude from high latitude with

reduced amplitudes due to the ion drag dissipation. The subsequent enhancements of ionospheric height can be associated with the strong eastward DD electric fields or TIDs as suggested by Lima et al. (2004), and Ram Singh and Sripathi. (2017, 2021).

3.3 Cross-correlation analysis between IEF and ionospheric parameters

The cross-correlation analysis technique can provide a measure of the similarity between different variables along with time delay. The range of cross-correlation coefficient varies from -1 to +1. The highest value of correlation between the compared parameters reflects by ±1, but moderate or poor correlation indicates by around zero. We used cross-correlation analysis technique to understand the causal relationship between solar wind parameters (e.g., IEFy) and ionospheric parameters (e.g., EEJ, H-component and VTEC). The horizontal component H of magnetic field (cf., northward in the equator) along the meridional chain of magnetometers can provide insights of the effects of the DP2 current system penetrating up to equatorial latitudes. The ΔH components are coherently fluctuating meridionally from high-mid to equatorial latitudes in good correlations with IMF Bz fluctuations so that H-components are enhanced when IMF Bz turns maximum in southward direction as shown in Figure S1 (provided as supplements).

Figure 7 shows residual variations (top panels) and cross-correlation (bottom panels) of (a) IEFy and H-components (at MGD, BMT, KNY, and GUA), (b) IEFy and EEJ, and (c) EEJ and VTEC (at BJFS, TCMC, and PIMO) during the main phase of storm from 22:00 UT on 03rd to 06:00 UT on 04th November. The residuals of all the parameters are extracted by using the 3rd order Savitzky-Golay smoothing algorithm (Savitzky and Golay, 1964).

In Figure 7a, the cross-correlation between the IEFy and H-components in MGD (black curve), BMT (green curve), and KNY (pink curve) shows good correlation with a correlation coefficient at 0.53 and a 0 time delay. In the meanwhile, the IEFy and H-component at the equatorial station (GUA) showed a maximum positive correlation coefficient of ~0.56 with a -12 min lag, which means that IEFy led the H-component 12 min before the equatorial magnetometer was triggered. In Figure 7b, IEFy and EEJ showed a maximum correlation coefficient of ~0.68 with a -12 min lag. In Figure 7c, the EEJ and VTEC at PIMO (blue curve) and TCMC (pink curve) reached positive correlations with maximum coefficients of ~0.34 and 0.63 (highest) and around zero lags, respectively; In the meanwhile, the EEJ and VTEC at BJFS (green curve) over mid latitude showed positive correlation with a maximum coefficient of

~0.40 with −7 min lag. As a result, the IEFy-H components and IEFy-EEJ gained good cross-correlations with ~0.53 and 0.68 correlation coefficients. This means that the modulations of H-components and EEJ can be associated as much as ~53% and 68% with IEFy fluctuations, respectively. The EEJ-VTEC correlation reflects that the fluctuations of VTEC at equatorial and low latitudes are moderately (~40%) affected by EEJ, while, at the mid latitude are well modulated (~68%) by EEJ.

3.4 Periodogram Analysis of Solar Wind/Ionospheric Parameters

To understand the causal relationship among the modulations of H-component of the magnetic field, ionospheric density (GPS-TEC and foF2) and height (h'F), and the oscillation of IEFy, we performed morlet wavelet analysis (Torrence and Compo, 1998). The fast and short fluctuating components are extracted by the Savitzk-Golay algorithm (Savitzky & Golay, 1964). Figure 8a shows the wavelet spectrum of ΔH-components at MGD (high latitude), MMB (mid latitude), KNY (low latitude) and GUA (equator). The wavelet spectrum of VTEC is shown in Figure 8b, from the top, for YAKT (high latitude), BJFS (mid latitude), TCMS (low latitude), and PIMO (equator). Figure 8c shows the wavelet spectrum of foF2 at Icheon (mid latitude), foF2 at Guam (low latitude), h'F at Guam, and IEFy. The white color dashed lines in the left panels show cones of influence; and in the right panel blue and red color lines depict the global wavelet spectrum (GWS) and 95% significant level, respectively. From the GWS, it is clear that a periodicity of ~1.05 hrs with FWHM (full width at half maximum) ~0.68-1.43 hrs is strongly dominant in H-components, VTEC, foF2, and h'F; and a dominant periodicity of ~0.9 hrs with of FWHM 0.5-1.3 hrs is obtained from IEFy. From the wavelet analysis, it is striking that the wavelet analysis finds a common and dominant periodic oscillation of ~1 hr period in the IEFy and ionospheric parameters. This analysis suggests that the perturbations of ionospheric density and magnetic field are the result of being modulated by quasi-periodically oscillating penetrating electric field or reorientation of the IMF Bz.

4. Discussion:

It is well known that the orientations of IMF Bz most strongly control the energy transfer into the magnetosphere-ionosphere system. During the southward turning of IMF Bz, enhanced magnetospheric convection electric field penetrates into the equatorial and low latitude ionospheres via the high-latitude DP2 current system (Nishida, 1968b; Araki et al., 1985;

Kikuchi et al., 1996; Huang 2019a, 2020), and significantly changes the electrodynamics and compositions in the lower latitude ionospheric regions (Kelley et al., 2004, Lima et all., 2004; Lin et al., 2005; Balan et al., 2010; Fagundes et al., 2016).

4.1 Ionospheric density modulation by PPEF and TID (or DDEF)

It is well known that the eastward and westward polarity of the electric field moves the F region height up and down. If the plasma gets pushed down too low in altitude, it leads to a depletion in the plasma density at the F region as a result of increased recombination with the neutrals. During the daytime, if the plasma does not come too low altitudes, the net plasma density of F layer height increases due to the minimal plasma loss by the recombination, less plasma diffusion along the field lines, and continued ion photoproduction (Tsurutani et al., 2008; Ambili et al., 2013; Shreedevi et al., 2017). Also, the enhancements/reductions of ionospheric plasma density can be found in the intensity and direction of disturbance winds as originated from Joule heating in the auroral region. The equatorward wind pushes the F layer height up, leading to thereby increasing of plasma density by less recombination and continuing photoionization.

The PP electric field-driven ionospheric perturbations usually occur instantaneously at different latitudes in the same longitudinal zone because of the quick penetration of magnetospheric electric fields from high to middle-low latitudes (Lima et al., 2004; Fagundes et al., 2016). However, the disturbed winds in association with TIDs or DDEF show time delay at different latitudes along the propagation direction due to the ion drag (Hocke and Schlegel, 1996; Hunsucker, 1982; Lee et al., 2004). In our observations, almost at the same time modulations in VTEC/foF2 at all latitudes, as seen in Figures 3-5, believed as driven by the PP electric fields (Lima et al., 2004; Fagundes et al., 2016). During the occurrence of multiple peaks in VTEC and foF2, the h'F should be changed either increased or decreased at all latitudes but don't show significant changes except for the equatorial station at GUA. This means there was no loss in the plasma density due to the minimal effect of recombination or plasma transport, and at the same time ion photoproduction continued, so there can be a net increase in foF2/VTEC without changing the F layer height (Lu et al., 2001; Lei et al., 2008).

Fagundes et al., (2016) have reported that the positive ionospheric peaks occurred simultaneously at mid and low latitude regions over the Brazilian sector on 17 March 2015. They suggested that the simultaneous enhancements of electron density peaks or wavelike

oscillations in electron density are strongly associated with PPEFs, but not by the traveling ionospheric disturbances (TIDs) or other sources.

Lima et al. (2004) distinguished the role of electric field from TIDs on the positive ionospheric storms along the meridional direction. They suggested that, in the case of TIDs, the perturbations are first observed at mid latitudes or beyond the EIA crest and then at low latitudes and finally at the equatorial region. However, as for the PP electric field, the positive ionospheric storm perturbations must simultaneously occur at all latitudes, since the PP electric field is on the global scale. During the recovery phase of the magnetic storm, on 04-05th November, enhancements and reductions in foF2 are due to DD electric fields or TIDs (Figure 5). The first peak in ionospheric density was observed at high latitude station and after ~2.5 hours occurred at the equator with propagation speed ~477 km/sec, as pointed out with blue color dashed line (in Figure 5). Since we see some correlation between one station and others with a time delay, we believe that they could be due to the TIDs or DDEFs. On 5 November, suppression of EIA crest or negative ionospheric storm at low latitudes may be linked to the DDEF (Figure 4).

4.2 h'F modulation by PPEF and TIDs (or DDEFs)

Ram Singh and Sripathi (2017) showed the simultaneous reductions/enhancements in h'F over the Indian region using a chain of ionosondes. They suggested that the ionospheric F region disturbances during the main phase of the storm are produced by the PPEF. It has been suggested that the super fountain effect during the geomagnetic storm is closely linked with PPEF and it leads to a stronger EIA (Lu et al., 2012; Abdu et al., 2007; Mannucci et al., 2005, Ram Singh et al., 2017). Our observations clearly show that EIA over the East Asian sector is significantly affected by the PPEF, and extending the enhanced electron density to higher latitudes without reflecting in the h'F at different latitudes in the same longitudinal zone except for the equatorial station at GUA. Meanwhile, several authors have also suggested that the storm time enhancement and suppression in the foF2 at midlatitudes are due to the change of thermospheric compositions (Prolss, 1977; Rishbeth, 1975), and wavelike disturbances in foF2 associated with high velocity TIDs or with substorm activity (Turunen and Mukunda Rao., 1980; Lima et al., 2004).

During geomagnetic storms, at the nightside, disturbed winds in association with TIDs can easily reach lower latitudes due to the least ion drag from low densities (Lu et al., 2001; Lei et

al., 2008). The equatorward wind lifts up the F layer height, leading to thereby decreasing plasma density by faster ion recombination and absence of photoionization, thereby an increase in F layer height and reduction in plasma density (Prolss, 1993; Rishbeth, 1975). During the recovery phase, between 12:00 and 22:00 UT (~21:00 and 06:00 LT) on 04 November, the significant enhancements in h'F could be associated with the DDEF or TIDs.

Sastri et al. (2000) presented the sharp reductions/enhancements of F layer height (h'F) at the same time at several stations over the Indian region, and suggested that reductions/enactments of F layer height are associated with the westward/eastward penetration electric fields. During the recovery phase of the magnetic storm, Figure 6 shows TID signature so that the first peaks of the h'F first observed at the high latitude stations and after ~2.5 hours reached at the equator, as pointed out with blue color dashed lines. Since we see a systematic enhancement along the h'F stations with a time delay (slope = 477 m/s), we believe that they could be associated with TIDs.

4.3 Evidence of oscillations of PPEF and DP2 current system

It is well established that the PPEF is linked to the region 1 (R1) and region 2 (R2) field-aligned currents and their horizontal closure currents, and they play an important role in generating the global scale ionospheric currents. When the FACs are in their dynamical activities, they can generate significant fluctuations in DP2 current systems that can easily penetrate to the equatorial region and modulate the electrodynamics of the ionosphere. Several studies have focused on the formations of quasi-periodic ionospheric current systems (Nishida, 1968b; Huang, 2019a, 2020), and solar wind magnetosphere-ionosphere coupling processes (Nishida, 1968b; Araki et al., 1985; Spiro et al., 1988; Kikuchi et al., 1996, 2008) and their impacts on the equatorial density distribution (Yizengaw et al., 2016; Shreedevi and Choudhary., 2017; Li et al., 2019). The quasi-periodic disturbances in ionospheric current systems are associated with various solar wind and magnetospheric processes (Gonzales et al., 1979; Nishida, 1968b; Kikuchi et al., 2000; Huang, 2019a, 2020). Nishida (1968b) reported the quasi-periodic oscillations in geomagnetic field measured by the ground-based magnetometers near the magnetic equator, caused by the penetration of electric fields associated with turning of IMF Bz with periods ~30-60 min. They suggested that during the turning of IMF Bz (north-south), the convection electric field and DP2 currents enhances and causes the magnetic fluctuations at the equator through the penetration electric field. Gonzales et al. (1979) and Earle and Kelley

(1987) reported the significant dominance of 1-hour periodicity in the IMF Bz as well in the electric fields at the auroral and equatorial latitudes. In our observations, magnetic field perturbations at high mid and low latitudes are well correlated with reorientations of IMF Bz (Figure S1) and show common and dominant periods ~30 to 90 min (Figure 8).

In a recent study, Huang (2019a) analyzed the observations of equatorial ionospheric plasma drift measured by the Jicamarca incoherent scatter radar and global ground magnetic field perturbations during IMF Bz fluctuations. Huang (2019a) also reported that the vertical plasma drifts/zonal electric fields in the dayside equatorial ionosphere are well correlated with reorientations of IMF Bz. Using the combination of ground-based magnetometers and EISCAT radar data, Kikuchi et al. (2000) showed a significant increase/decrease of the DP2 current system at high latitude and EEJ at the equator, according to sudden polarity changes of IMF Bz from north-south/south-north. They suggested that when IMF Bz turns north-south/south-north both the DP2 current system and EEJ get enhanced/decayed, and eastward/westward electric field enhanced/reduced at the equator. The correlations coefficient of IEFy with EEJ and H-components is 0.68 and 0.53, respectively, suggesting that the IEFy is playing an important role in electric field penetration down to the equatorial region. Our observations show excellent time coincidence between the IMF Bz minimum and H-components peaks (Figure S1), the H-components enhanced when IMF Bz turns maximum in southward direction which are consistent results as presented in the previous studies (Kikuchi et al., 2000; Yizengaw et al., 2016; Huang, 2019a, 2020).

In general, the vertical motion of the ionosphere is driven by the eastward/westward electric field at the equator, which generates due to the turning of IMF Bz. As shown in Figure 7, the correlation of a latitudinal array of H-components with IMF Bz can be an evidence of the modulated DP2 currents to be effective on all the latitudes in the longitudinal sector. Given this correlation, the coherent fluctuations of the VTEC/foF2 (in Figures 3 and 5) can be the signatures in the lower latitude ionosphere affected by the modulated DP2 current system. Figure 6 shows that the virtual height of the ionosphere is not showing pronounced effect of storm at all latitudes, but oscillating up and down compared to mean variation at equatorial and low latitudes, implying that the DP2 current fluctuations control the ionospheric F-layer height. This can be demonstrate that the magnetospheric origin quasi-periodic electric field can penetrate to the ionosphere and drive DP2 current fluctuations that extend to the lower latitude

ionosphere and create significant effects on the ionospheric density distribution by making the F layer move up and down. The correlation between the magnetospheric origin electric fields measured by the ground-based magnetometers and those by radars during magnetic storm periods have been performed (Kelley et al., 2007; Yizengaw et al., 2016; Huang, 2019a, 2020). In addition, several researchers have reported a wide range of periodicities of ~0.5 to 2 hours associated with the DP2 current system (Nishida , 1968b; Gonzales et al., 1979; Earle and Kelley, 1987; Sastri et al., 2002; Chakrabarty et al. 2008; Huang, 2019a). Nonetheless, we report that the solar wind magnetosphere-ionosphere interactions-driven DP 2 current systems can modulate ionospheric density not only at the equatorial latitude, as did by Yizengaw et al. (2016), but also, for the first time, at high-mid and low latitudes. Based on the wavelet analysis we also report a dominant periodicity of ~1 hr VTEC, foF2, and H-component, which are driven by the PP electric field associated with the DP2 current system due to IMF Bz. This suggests a causal relationship exists among IEF, DP2 current system, and ionospheric density oscillations at all latitudes.

5. Conclusions

This study observed the meridional ionospheric density responses to prompt penetration electric field (PPEF) over the East Asian sector, during an intense geomagnetic storm that occurred on November 3-5, 2021 in the current solar cycle 25. The important findings of the investigation can be summarized as follows:

(1) The VTEC and foF2 observations demonstrated that repeated positive ionospheric storms can be associated with reorientations of IMF Bz or DP2 current systems.

(2) From the time-latitude map of TEC observation, the equatorial ionization anomaly (EIA) is significantly disturbed during the main phase, and the signature of repeated positive ionospheric storms are observed. It is remarkable that three peaks of VTEC/foF2 with large amplitudes are extended from the equator to high latitudes simultaneously without wave propagation signatures. The first peak occurred at 6.67^{o} S-43.79^{o} N, the second peak with a large amplitude in the extended latitude range of 6.67^{o} S-62.03^{o} N, and the third peak in 14.67^{o} S-71.63.79^{o} N.

(3) In the recovery phase, enhancements/reductions in foF2 and h'F are associated with the disturbance dynamo (DD) electric field or traveling ionospheric disturbances (TIDs).

(4) The periodogram analysis and wavelet spectra show dominant and common periods of ~1 hour among VTEC, H-component, foF2, h'F, and IEFy.

We conclude that the modulations of VTEC, foF2 and H-component during the main phase of geomagnetic storm can be driven by the PP electric field associated with DP2 current system and IMF Bz, and in the recovery phase, the response of VTEC from equatorial to mid latitudes can be driven by DD electric field or TIDs. The common and dominant periodicity of 1hr in all the ionospheric parameters and IEF suggests that a causal relationship exists among IEF, DP2 current system, and ionospheric density modulations at all latitudes.

Acknowledgments

This work was supported by the National Research Foundation of Korea (NRF) grant funded by the Korea government (MSIP) (No. 2021R1A2C1005306). We acknowledge use of NASA/GSFC's Space Physics Data Facility's OMNIWeb (or CDAWeb or ftp) service, and OMNI data used in this study. The VTEC-GPS data were obtained through the online archives of the Crustal Dynamics Data Information System (CDDIS), NASA Goddard Space Flight Center, Greenbelt, MD, USA, and from MIT Haystack Observatory Madrigal database. This publication makes use of data from Ionosonde stations, owned by Institute of Geology and Geophysics, Chinese Academy of Sciences (IGGCAS) and supported in part by Solar-Terrestrial Environment Research Network of CAS and Meridian Project of China and USAF NEXION Digisonde network.

References

Abdu, M. A., Maruyama, T., Batista, I. S., Saito, S., & Nakamura, M. (2007). Ionospheric responses to the October 2003 superstorm: Longitude/local time effects over equatorial low and middle latitudes. *J. Geophys. Res.*, 112, A10306. https://doi.org/10.1029/2006JA012228.

Abdu, M. A., Sastri, J. H. et al. (1998). DP 2 electric field fluctuations in the dusk-time dip equatorial ionosphere. *Geophys. Res. Lett.*, 25(9), 1511–1514.

Ambili, K. M., Choudhary, R. K., Maurice, J.-P. S., & Chau, J. (2013). Nighttime vertical plasma drifts and the occurrence of sunrise undulation at the dip equator: A study using Jicamarca incoherent backscatter radar measurements. *Geophys. Res. Lett., 40*, 5570–5575. https://doi.org/10.1002/2013GL057837.

Araki, T., J. H. Allen, & Y. Araki (1985). Extension of a polar ionospheric current to the night side equator. *Planet. Space Sci.*, 33(1), 11–16.

Balan, N., K. Shiokawa, Y. Otsuka, et al. (2010). A Physical mechanism of positive ionospheric storms at low and mid latitudes through observations and modelling. *J. Geophys. Res.*, 115, A02304, doi:10.1029/ 2009JA014515.

Blanc & Richmond (1980). the ionospheric disturbances dynamo. *J. Geophys. Res.*, 85, 1669.

Chakrabarty, D., R. Sekar, J. H. Sastri, & S. Ravindran (2008). Distinctive effects of interplanetary electric field and substorm on nighttime equatorial F layer: A case study. *Geophys. Res. Lett.*, 35 (19), 307 doi:10.1029/2008GL035415, l19108.

Clauer, C. R., & Y. Kamide (1985). DPl and DP2 current systems for the March 22, 1979 substorms. *J. Geophys. Res.*, 90, 1343–1354.

Earle & Kelley (1987). Electric Field Strength, Fourier Analysis, Incoherent Scatter Radar, Ionospheric Currents, Spectrum Analysis, Gravity Waves, Periodic Variations, Plasma Drift. *J. Geophys. Res.*, 10.1029/JA092iA01p00213.

Fagundes, P. R., F. A. Cardoso, B. G. Fejer, et al. (2016). Positive and negative GPS-TEC ionospheric storm effects during the extreme space weather event of March 2015 over the Brazilian sector. *J. Geophys. Res.*, 121, 5613–5625, doi:10.1002/2015JA022214.

Fujiwara, H., Maeda, S., Fukunishi, H., Fuller-Rowell, T.J., & Evans, D.S. (1996). Global variations of thermospheric winds and temperatures caused by substorm energy injection. *J. Geophys. Res.*, 101, 225–239.

Fuller-Rowell, T. J., Codrescu, M. V., Rishbeth et al. (1996). On the seasonal response of the thermosphere and ionosphere to geomagnetic storms. *J. Geophys. Res.*, 101(A2):2343-2353.

589 Gaunt, C. T. & Coetzee, G. (2007). Transformer failures in regions incorrectly considered to
590 have low GIC-risk. *IEEE Lausanne Power Tech*, pp. 807-812, doi:
591 10.1109/PCT.2007.4538419.
592 Goncharenko, L. P., J. C. Foster, A. J. Coster, C. Huang, N. Aponte, & L. J. Paxton (2007).
593 Observations of a positive storm phase on 10 September 2005. *J. Atmos. Sol. Terr. Phys.,* 69
594 (10–11), 1253–1272, doi: 10.1016/j.jastp.2006.09.011.
595 Gonzales, C. A., Kelley, M. C., & Woodman, R. F. (1979). Equatorial electric fields during
596 magnetically disturbed conditions: Implications of simultaneous auroral and equatorial
597 measurements. *J. Geophys. Res.,* 84, 5803–5812.
598 Hocke, K., & K. Schlegel (1996). A review of atmospheric gravity waves and traveling
599 ionospheric disturbances: 1982–1995, *Ann. Geophys.,* 14, 917–940.
600 Huang, C.-S. (2019a). Global ionospheric current system associated with penetration electric
601 field and new mechanism for the generation of dayside westward electric field at low latitudes
602 during northward IMF. *J. Geophys. Res.,* 124, 3827–3842.
603 https://doi.org/10.1029/2018JA026345.
604 Huang, C.-S. (2020). Systematical analyses of global ionospheric disturbance current systems
605 caused by multiple processes: Penetration electric fields, solar wind pressure impulses,
606 magnetospheric substorms, and ULF waves. *J. Geophys. Res.,* 125, e2020JA027942.
607 https://doi.org/10.1029/2020JA027942.
608 Hunsucker, R. D. (1982). Atmospheric gravity waves generated in the high latitude ionosphere:
609 A review, *Rev. Geophys.,* 20 (2), 293– 315, doi:10.1029/RG020i002p00293.
610 Joshi, L. M., S. Sripathi, & R. Singh (2016). Simulation of low-latitude ionospheric response
611 to 2015 St. Patrick's Day super geomagnetic storm using ionosonde-derived PRE vertical
612 drifts over Indian region. *J. Geophys. Res.,* 121, 2489–2502, doi:10.1002/2015JA021512.
613 Kelley, M. C., Fejer, B. G., & Gonzalez, C. A. (1979). An explanation for anomalous equatorial
614 ionospheric electric fields associated with the northward turning of the interplanetary
615 magnetic field. *Geophys. Res. Lett.,* 6(4), 301–304.
616 Kelley, M. C., M. J. Nicolls, et al. (2007). Multi-longitude case studies comparing the
617 interplanetary and equatorial ionospheric electric fields using an empirical model. *J. Atmos.*
618 *Terr. Phys.,* 69(10–11), 1174–1181, doi: 10.1016/j.jastp.2006.08.014.

619 Kelley, M. C., M. N. Vlasov, J. C. Foster, & A. J. Coster (2004). A quantitative explanation for
620 the phenomenon known as storm-enhanced density. *Geophys. Res. Lett.*, 31, L19809,
621 doi:10.1029/2004GL020875.
622 Kikuchi, T., K. K. Hashimoto, & K. Nozaki (2008). Penetration of magnetospheric electric
623 fields to the equator during a geomagnetic storm. *J. Geophys. Res.*, 113, A06214,
624 doi:10.1029/2007JA012628.
625 Kikuchi, T., Luhr, H. et al. (2000). Penetration of auroral electric fields to the equator during a
626 substorm. *J. Geophys. Res.*, 105(A10), 23,251–23, 261.
627 Kikuchi, T., Lühr, H., Kitamura, T. et al. (1996). Direct penetration of the polar electric field
628 to the equator during a DP 2 event as detected by the auroral and equatorial magnetometer
629 chains and the EISCAT radar. *J. Geophys. Res.*, 101(A8), 17,161–17,173.
630 Lee, C. C., J. Y. Liu, M. Q. Chen, S. Y. Su, H. C. Yeh, & K. Nozaki (2004). Observation and
631 model comparisons of the traveling atmospheric disturbances over the Western Pacific region
632 during the 6–7 April 2000 magnetic storm. *J. Geophys. Res.*, 109, A09309,
633 doi:10.1029/2003JA010267.
634 Lei, J., Burns, A. G., Tsugawa, T., Wang, W., Solomon, S. C., and Wiltberger, M. (2008).
635 Observations and simulations of quasiperiodic ionospheric oscillations and large-scale
636 traveling ionospheric disturbances during the December 2006 geomagnetic storm. *J. Geophys.*
637 *Res.*, 113, A06310, doi:10.1029/2008JA013090.
638 Lima, W. L. C., F. Becker-Guedes, et al. (2004). Response of the equatorial and low-latitude
639 ionosphere during the space weather events of April 2002. *Ann. Geophys.*, 22(9), 3211–3219,
640 doi:10.5194/angeo-22-3211-2004.
641 Lin, C. H., A. D. Richmond, R. A. Heelis, G. J. Bailey, G. Lu, J. Y. Liu, H. C. Yeh, & S. Y. Su
642 (2005). Theoretical study of the low-and midlatitude ionospheric electron density
643 enhancement during the October 2003 storm: Relative importance of the neutral wind and the
644 electric field. *J. Geophys. Res.*, 110, A12312, doi:10.1029/2005JA011304.
645 Liu, C. M., L. G. Liu, R. Pirjola, & Z. Z. Wang (2009). Calculation of geomagnetically induced
646 currents in mid- to low-latitude power grids based on the plane wave method: A preliminary
647 case study. *Space Weather*, 7, S04005, doi:10.1029/2008SW000439.
648 Liu, J., L. Liu, T. Nakamura, B. Zhao, B. Ning, & A. Yoshikawa (2014). A case study of
649 ionospheric storm effects during long-lasting southward IMF Bz-driven geomagnetic storm.
650 *J. Geophys. Res.* 119, 7716–7731, doi:10.1002/2014JA020273.

651 Lu, G., Richmond, A. D., Roble, R. G., and Emery, B. A. (2001). Coexistence of ionospheric
652 positive and negative storm phases under northern winter conditions: A case study. *J. Geophys.*
653 *Res.*, 106(A11), 24493– 24504, doi:10.1029/2001JA000003.
654 Nishida, A. (1968b). Coherence of geomagnetic DP 2 fluctuations with interplanetary magnetic
655 variations. *J. Geophys. Res.,* 73(17), 5549–5559, doi: 10.1029/JA073i017p05549.
656 Noll, C.E. (2010). The Crustal Dynamics Data Information System: A resource to support
657 scientific analysis using space geodesy. *Adv. Space Res.* 2010, 45, 1421–1440.
658 Prolss, G. W. (1993). Common origin of positive ionospheric storms at middle latitudes and
659 the geomagnetic activity effect at low latitudes. *J. Geophys. Res.*, 98(A4):5981–5991.
660 Prolss, G. W., and M. J. Jung (1978). Traveling atmospheric disturbances as a possible
661 explanation for daytime positive storm effects of moderate duration at middle latitudes. *J.*
662 *Atmos. Terr. Phys.*, 40, 1351 – 1354.
663 Prolss, G., Roemer, M., & Slowey, J. (1988). Dissipation of solar wind energy in the earth's
664 upper atmosphere: The geomagnetic activity effect. *Adv. Space Res.*, (5-6):215-261.
665 Ram Singh & Sripathi, S. (2021). The role of storm-time electrodynamics in the dawn and dusk
666 sectors across equatorial and low-latitude ionosphere during December 19–21, 2015. *J.*
667 *Geophys. Res.,* 126, e2020JA029072.
668 Ram Singh, S. Sripathi, et al., (2015). Low-latitude ionosphere response to super geomagnetic
669 storm of 17/18 March 2015: Results from a chain of ground based observations over Indian
670 sector. *J. Geophys. Res.,* 120, 10,864–10,882.
671 Ram Singh., & Sripathi, S. (2017). Ionospheric response to 22–23 June 2015 storm as
672 investigated using ground-based ionosondes and GPS receivers over India. *J. Geophys. Res.,*
673 122, 11,645–11,664. 2017JA024460.
674 Reddy, C. A., Nishida, A., Fukao, S., & Somayajulu, V. V. (1990). Magnetospheric substorm
675 related electric fields in the ionosphere: Discrepancy of an observation with model predictions.
676 *Geophys. Res. Lett.,* 17(13):2333–2336.
677 Rishbeth, H. (1975). F-region storms and thermospheric circulation. *J. Atmos. Sol. Terr. Phys.,*
678 37, 1055–1064. https://doi. org/10.1016/0021-9169(75)90013-6.
679 Rishbeth, H. (1998). How the thermospheric circulation affects the ionospheric F2 layer. *J.*
680 *Atmos. Sol. Terr. Phys.*, 60(14):1385–1402.
681 Rishbeth, H. (2000). The equatorial F-layer: progress and puzzles, Ann. Geophys. 18, 730–739.

682 Rout, D., K. Pandey, D. Chakrabarty, R. Sekar, & X. Lu (2019). Significant Electric Field
683 Perturbations in Low Latitude Ionosphere due to the Passage of Two Consecutive ICMEs
684 During 6-8 September 2017. *J. Geophys. Res.*, 124 (11), 9494–9510,
685 doi:10.1029/2019JA027133.
686 Sastri, J. H., Jyoti, N., Somayajulu, V. V., Chandra, H., & Devasia, C. V. (2000). Ionospheric
687 storm of early November 1993 in the Indian equatorial region. *J. Geophys. Res.*, 105, 18,443–
688 18,455. https://doi.org/10.1029/1999JA000372.
689 Sastri, J. H., Niranjan, K., & Subbarao, K. S. V. (2002). Response of the equatorial ionosphere
690 in the Indian (midnight) sector to the severe magnetic storm of July 15, 2000. *Geophys. Res.*
691 *Lett.*, 29(13), 1651.10.10292002/2002GL015133.
692 Savitzky, A., & Golay, M. J. E. (1964). Smoothing and differentiation of data by simplified
693 least squares procedures. *Analytical Chemistry*, 36, 1627– 1639.
694 doi.org/10.1021/ac60214a047.
695 Shreedevi, P. R., & Choudhary, R. K. (2017). Impact of oscillating IMF Bz during 17 March
696 2013 storm on the distribution of plasma over Indian low-latitude and mid-latitude
697 ionospheric regions. *J. Geophys. Res.*, 122, 11,607–11,623.
698 Spiro, R. W., Wolf, R. A., & Fejer, B. G. (1988). Penetration of high-latitude-electric-field
699 effects to low latitudes during SUNDIAL 1984. *Annales de Geophysique*, 6, 39–50.
700 Torrence, C., and G. P. Compo (1998). a practical guide to wavelet analysis, Bull. *Am. Meteorol.*
701 *Soc.*79, 61-78.
702 Tsurutani, B. T., et al. (2008). Prompt penetration electric fields (PPEFs) and their ionospheric
703 effects during the greatmagnetic storm of 30 – 31 October 2003, *J. Geophys. Res.*, 113,
704 A05311, doi:10.1029/2007JA012879.
705 Yizengaw, E., Moldwin, M. B., Zesta, E., Magoun, M., Pradipta, R., Biouele, C. M., Rabiu, A.
706 B., Obrou, O. K., Bamba, Z., & de Paula, E. R. (2016). Response of the equatorial ionosphere
707 to the geomagnetic DP 2 current system. *Geophys. Res. Lett.*, 43, 7364– 7372,
708 doi:10.1002/2016GL070090.
709 Zhao, B., Wan, W., Lei, J., Wei, Y., Sahai, Y., & Reinisch, B. (2012). Positive ionospheric
710 storm effects at Latin America longitude during the superstorm of 20–22 November 2003:
711 Revisit. *Annales de Geophysique*, 30, 831–840.
712
713

Figures:

Figure 1. The location of various stations and instruments used in present study, (a) locations of GPS receivers, and Ionosondes, and (b) magnetometers.

Figure 2. Variation of interplanetary and geomagnetic conditions during the 03-05 November 2021. (a) Particle density (Np (cm^{-3})), black) and solar wind pressure (Pdyn (nPa)), red), (b) solar wind velocity (m/sec), (c) IMF By (blue) and Bz (red) in nT, (d) IEFy (mV/m), (e) Dst (nT), (f) EEJ (nT), and (g) Kp index. The black color shaded region indicates the main phase of the storm.

Figure 3. The VTEC diurnal variations (red solid lines) over the East Asian sector during the 03-05 November. The grey shaded region and solid black lines show IQDs mean and the averaged standard deviation. The vertical dotted blue color lines indicate the VTEC enhancements. The p1, p2 and p3 represent positive ionospheric storms. The n1 and n2 indicate negative ionospheric storms.

Figure 4. Shows (a) latitudinal and temporal variations of TEC (contour map); (b) ΔTEC = (TEC-TEC_{IQDs} Mean); TEC_{IQDs} Mean is five IQDs variations during the November month, over the Asian sector between 110-150^{o} E longitude.

Figures 5. Temporal variation of foF2 at (a) MH, (b) BP, (c) ICN, (d) JJ, (e) WU, (f) SA, and (g) GUA. The grey color lines with error bars indicate the quiet days mean and standard deviation. The vertical shaded green and blue color indicate the simultaneous enhancements in foF2.

Figures 6. Variations of h'F at (a) MH, (b) BP, (c) ICN, (d) WU, and (e) GUA. The grey color lines with error bars indicate the quiet days mean and standard deviation. The dashed blue color lines indicate the enhancements in h'F.

Figure 7. Infiltration of PPEF effects examined with cross-correlation analysis: Residual variations (top panels) and cross-correlation (bottom panels) of (a) IEFy and H-components (at MGD, BMT, KNY, and GUA), (b) IEFy and EEJ, and (c) EEJ and VTEC (at BJFS, TCMC, and PIMO) during 03-04 November 2021.

Figure 8. Wavelet spectrum analysis of (a) H-components of magnetic field at MGD, MMB KNY and GUA stations (top to bottom); (b) VTEC at YAKT, BJFS, TCMS and PIMO (top to bottom); and (c) foF2 ate Icheon (mid latitude) and Guam (low latitude), h'F at Guam, and IEFy (bottom panel). The dotted white color lines in each plot indicate cone of influence

(COI). The rightside panels of each plot show global wavelet spectrum (GWS) with 95% confidence level (in red color).

Table 1. Details of the GPS TEC stations, Ionosondes, SuperDARN and Magnetometers with name, station code, latitudes and longitudes

Location	Station CODE	Geographic (Latitude)	Geographic (Longitude)	Geomagnetic (Latitude)	Geomagnetic (Longitude)
GPS Receivers					
Tixi	TIXI	71.63º N	128.86º E	61.94º N	165.77º W
Yakutsk	YAKT	62.03º N	129.68º E	53.06º N	162.64º W
Changchun	CHAN	43.79º N	125.44º E	34.64º N	164.12º W
Fangshan	BJFS	39.60º N	115.89º E	30.14º N	172.39º W
Suwon-shi	SUWN	37.27º N	127.05º E	28.23º N	162.15º W
Daejeon	DAEJ	36.39º N	127.37º E	27.36º N	161.86º W
Hsinchu	TCMC	24.79º N	120.98º E	15.53º N	167.13º W
Hong kong	HKWS	22.43º N	114.33º E	13.00º N	173.35º W
Quezon City	PIMO	14.63º N	121.07º E	05.43º N	166.64º W
Lae	LAE	-06.67º N	146.99º E	13.78º S	139.25º W
Ionosondes					
Mohe	MH	52.00º N	122.52ºE	42.73ºN	167.26ºW
Beijing	BP	40.30ºN	116.20ºE	30.85ºN	172.10ºW
I-cheon	IC	37.14º N	127.54º E	28.11º N	161.76º W
Jeju	JJ	33.43º N	126.30º E	24.36º N	162.64º W
Wuhan	WU	30.50ºN	114.40ºE	21.04ºN	173.46ºW
Sanya	SA	18.53ºN	109.61ºE	8.87ºN	177.99ºW
Guam	GUA	13.69º N	144.87º E	6.12º N	143.44º W
Magnetometers					
Magadan	MGD	60.05º N	150.72º E	53.32º N	139.34º W
Paratunka	PET	52.97º N	158.20º E	46.36º N	137.17º W
Memambetsu	MMB	43.91º N	144.19º E	36.01º N	147.59º W
Beijing MingTombs	BMT	40.30º N	116.20º E	30.85º N	172.10º W
Gangneung	GANG	37.75º N	128.87º E	28.39º N	161.01º W
Ichoen	ICN	37.14º N	127.54º E	27.74º N	161.78º W
Kakioka	KAK	36.23º N	140.18º E	28.04º N	150.20º W
Jeju	JEJU	33.43º N	126.30º E	24.15º N	162.81º W
Kanoya	KNY	21.42º N	130.80º E	12.66º N	157.64º W
Guam	GUA	13.69º N	144.87º E	06.12º N	143.44º W

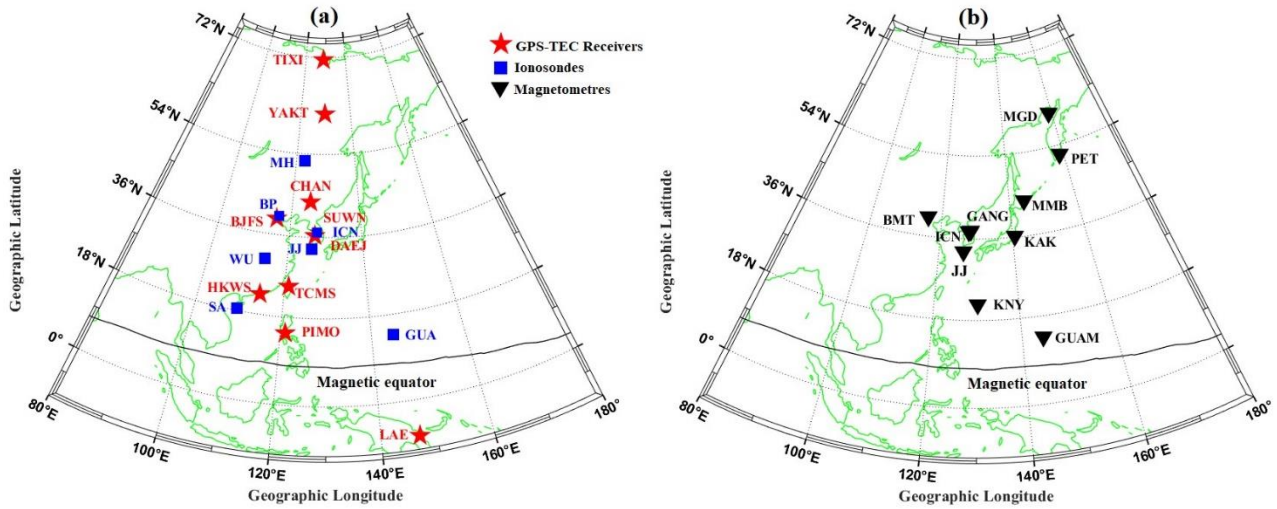
(a)
GPS-TEC Receivers
Ionosondes
Magnetometres
TIXI
YAKT
MH
CHAN
BP
BJFS
SUWN
ICN
DAEJ
JJ
WU
HKWS
ICMS
SA
PIMO
GUA
LAE
Magnetic equator
Geographic Latitude
Geographic Longitude
72°N
54°N
36°N
18°N
0°
80°E
100°E
120°E
140°E
160°E
180°
(b)
MGD
PET
MMB
BMT
GANG
ICN
KAK
JJ
KNY
GUAM
Magnetic equator
Geographic Latitude
Geographic Longitude

Figures 1 (a-b)

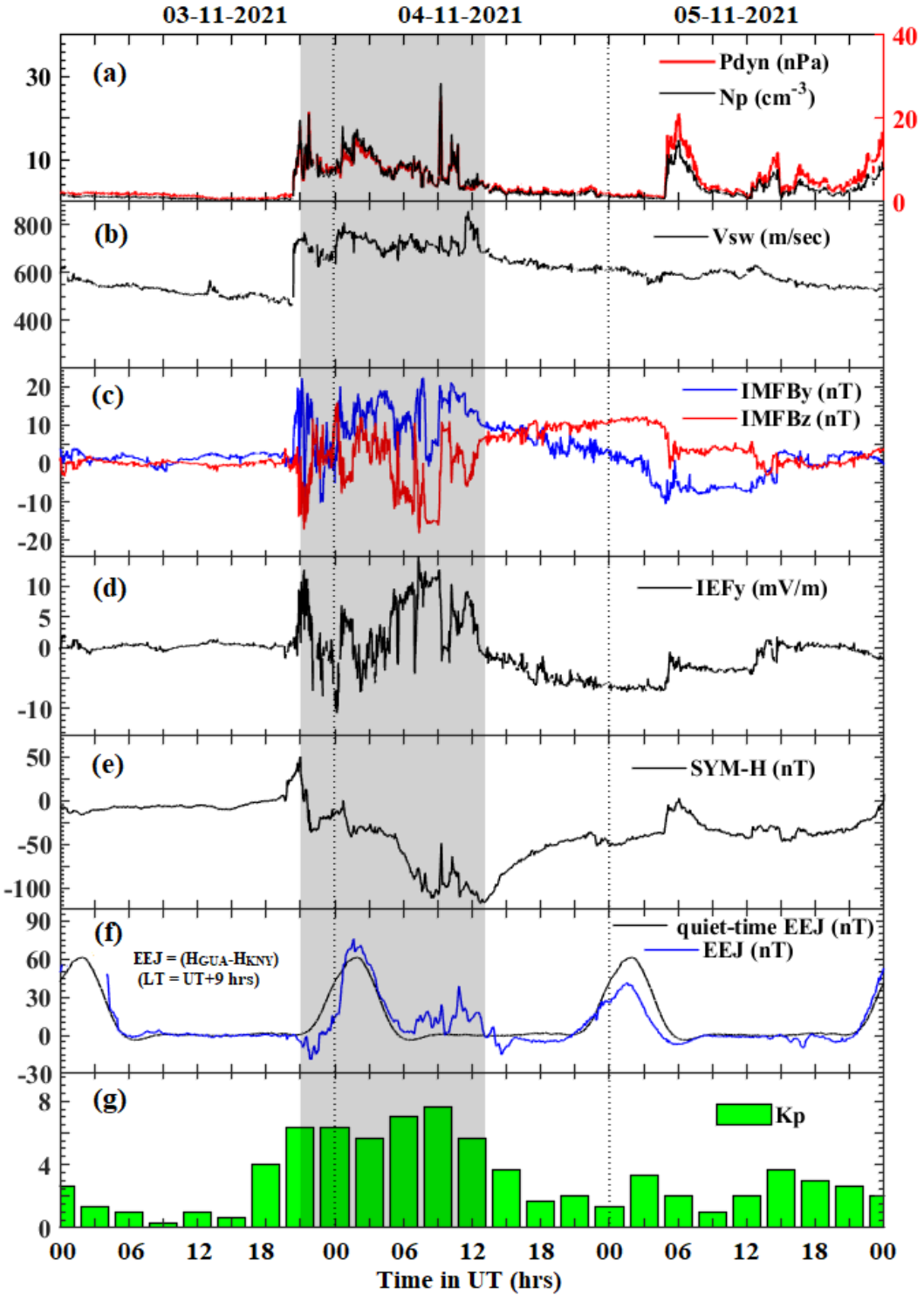
03-11-2021
04-11-2021
05-11-2021
(a)
Pdyn (nPa)
Np (cm-3)
(b)
Vsw (m/sec)
(c)
IMFBy (nT)
IMFBz (nT)
(d)
IEFy (mV/m)
(e)
SYM-H (nT)
(f)
quiet-time EEJ (nT)
EEJ (nT)
EEJ = (HGUA-HKNY)
(LT = UT+9 hrs)
(g)
Kp
Time in UT (hrs)

Figures 2 (a-g)

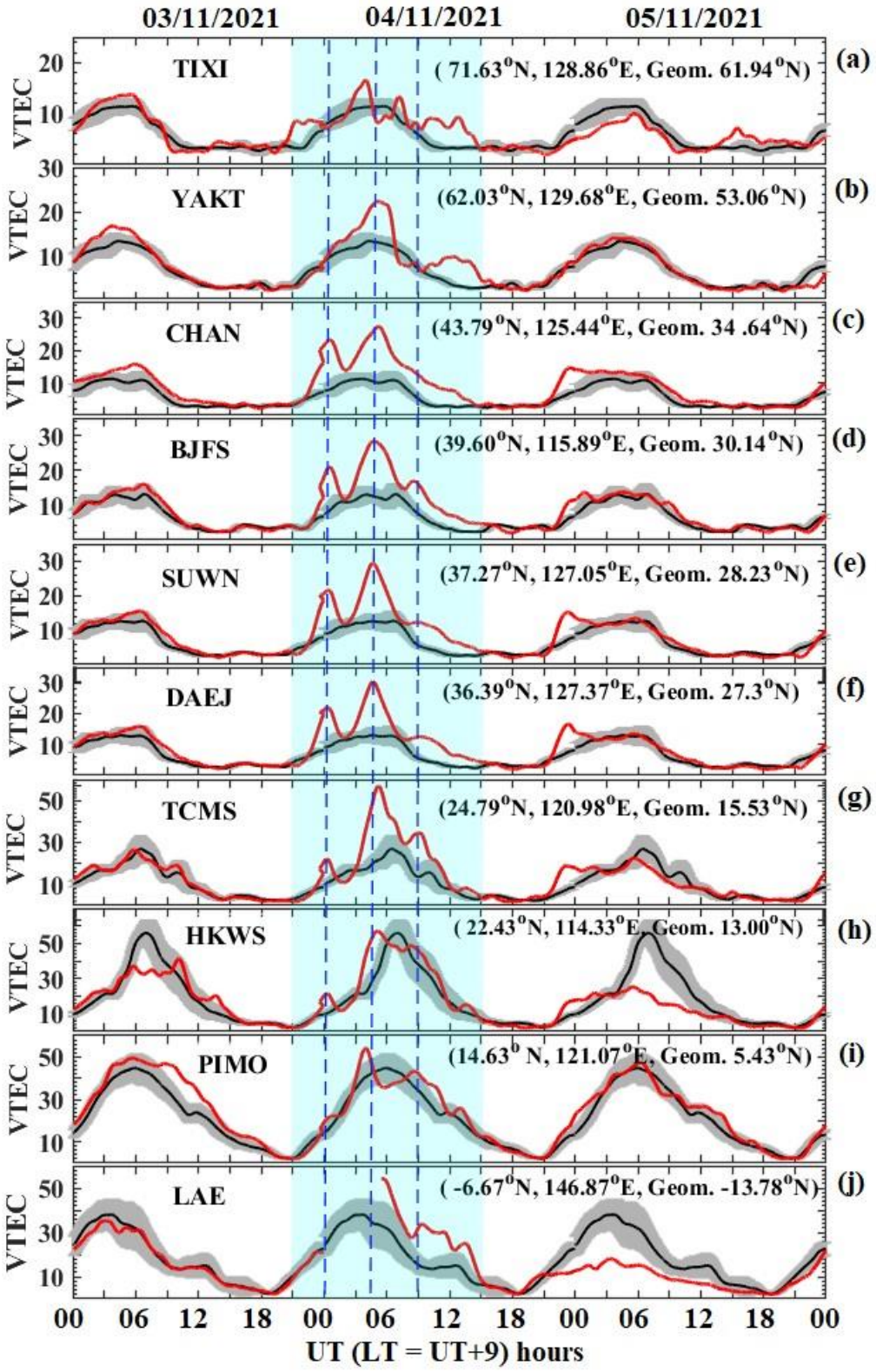
03/11/2021
04/11/2021
05/11/2021
TIXI
(71.63°N, 128.86°E, Geom. 61.94°N)
(a)
YAKT
(62.03°N, 129.68°E, Geom. 53.06°N)
(b)
CHAN
(43.79°N, 125.44°E, Geom. 34 .64°N)
(c)
BJFS
(39.60°N, 115.89°E, Geom. 30.14°N)
(d)
SUWN
(37.27°N, 127.05°E, Geom. 28.23°N)
(e)
DAEJ
(36.39°N, 127.37°E, Geom. 27.3°N)
(f)
TCMS
(24.79°N, 120.98°E, Geom. 15.53°N)
(g)
HKWS
(22.43°N, 114.33°E, Geom. 13.00°N)
(h)
PIMO
(14.63b N, 121.07°E, Geom. 5.43°N)
(i)
LAE
(-6.67°N, 146.87°E, Geom. -13.78°N)
(j)
VTEC
00 06 12 18 00 06 12 18 00 06 12 18 00
UT (LT = UT+9) hours

Figure 3 (a-j)

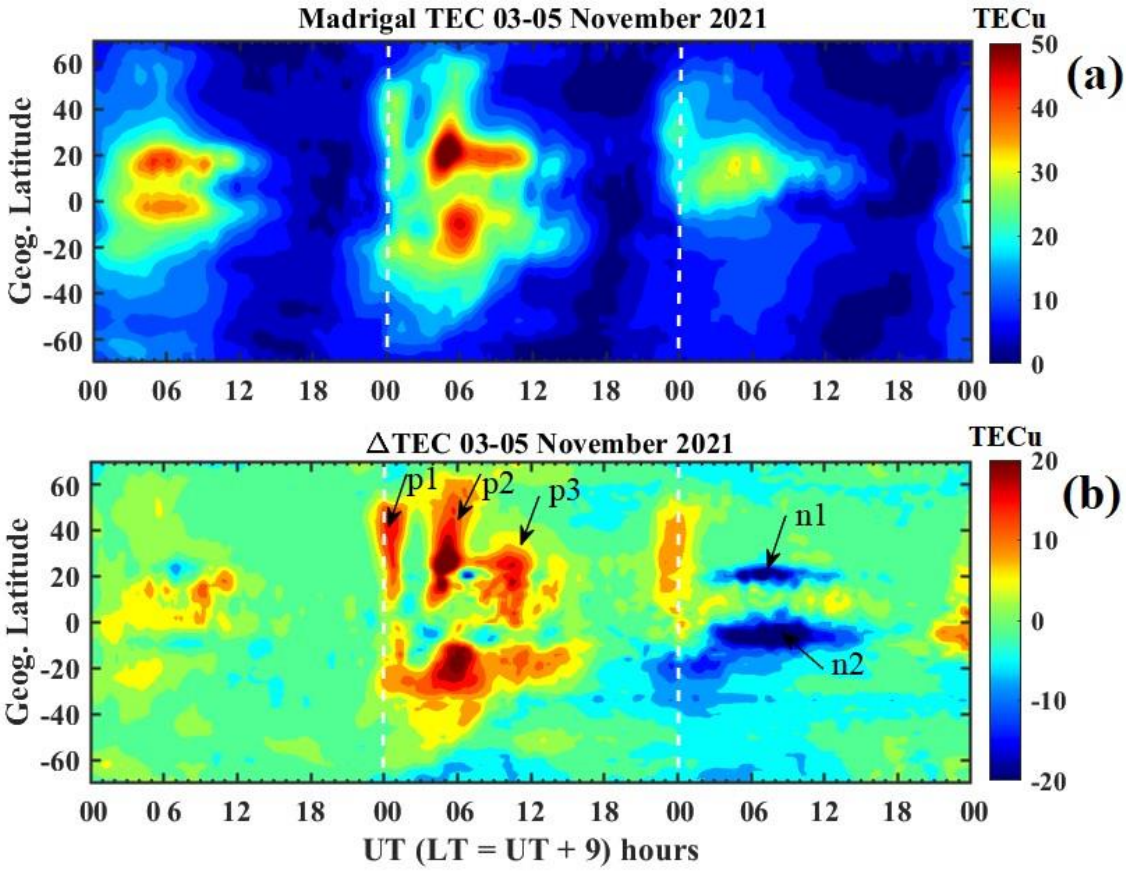
Madrigal TEC 03-05 November 2021
TECu
(a)
Geog. Latitude
ΔTEC 03-05 November 2021
TECu
(b)
p1
p2
p3
n1
n2
UT (LT = UT + 9) hours

Figure 4 (a-b)

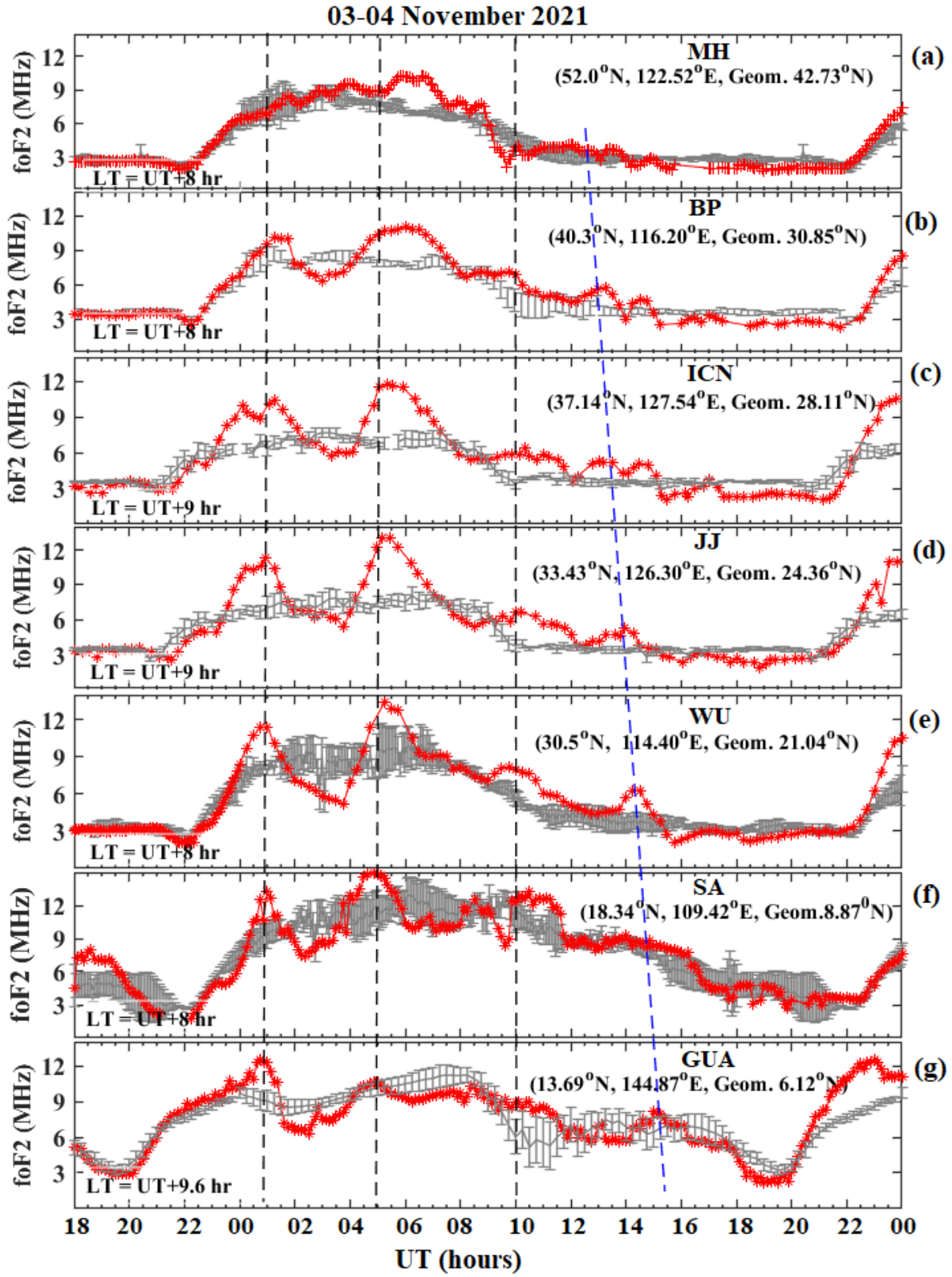
03-04 November 2021
MH
(52.0°N, 122.52°E, Geom. 42.73°N)
(a)
BP
(40.3°N, 116.20°E, Geom. 30.85°N)
(b)
ICN
(37.14°N, 127.54°E, Geom. 28.11°N)
(c)
JJ
(33.43°N, 126.30°E, Geom. 24.36°N)
(d)
WU
(30.5°N, 114.40°E, Geom. 21.04°N)
(e)
SA
(18.34°N, 109.42°E, Geom.8.87°N)
(f)
GUA
(13.69°N, 144.87°E, Geom. 6.12°N)
(g)
foF2 (MHz)
LT = UT+8 hr
LT = UT+9 hr
LT = UT+9.6 hr
UT (hours)

Figure 5 (a-g)

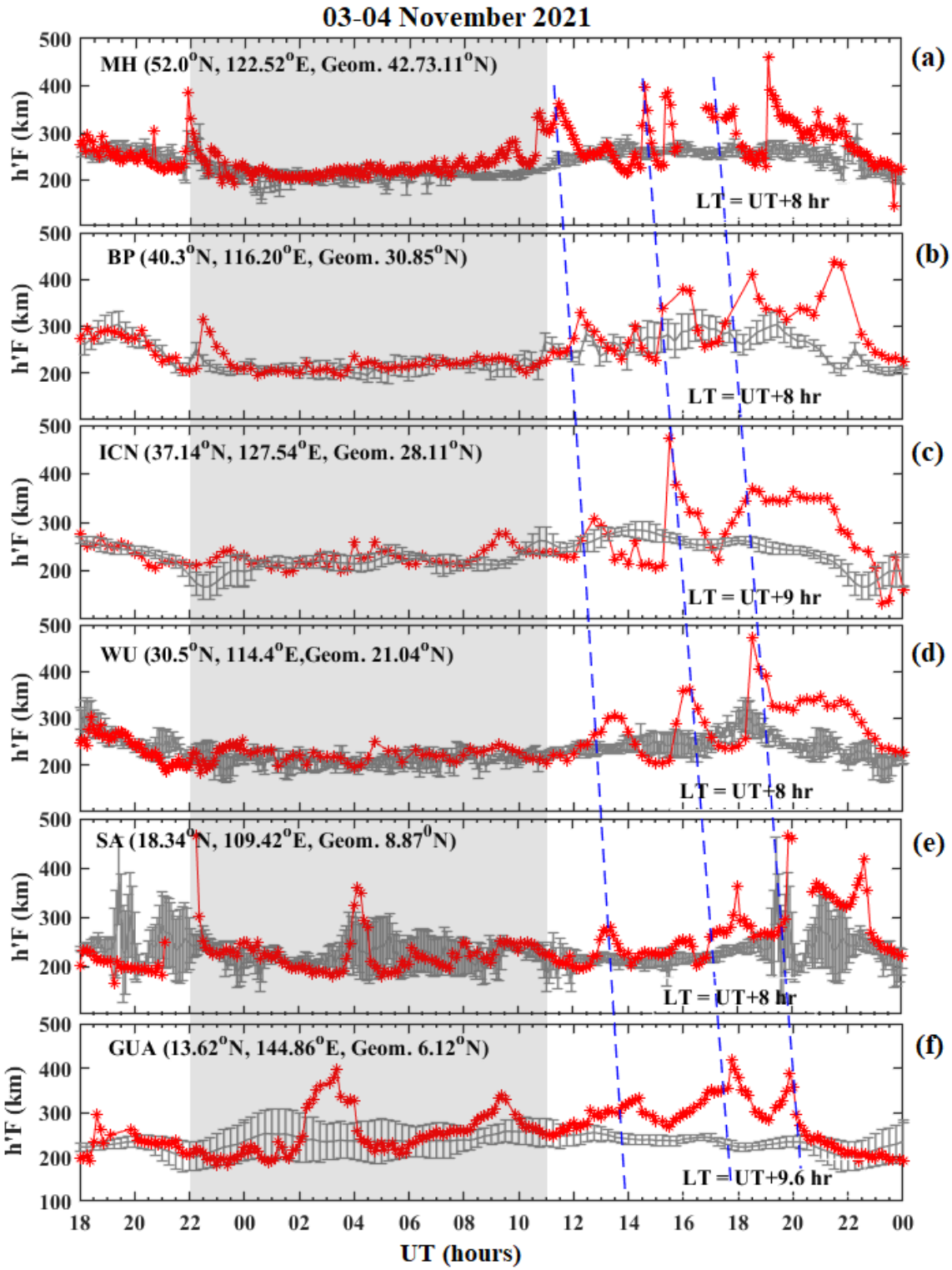
03-04 November 2021
MH (52.0°N, 122.52°E, Geom. 42.73.11°N)
(a)
LT = UT+8 hr
BP (40.3°N, 116.20°E, Geom. 30.85°N)
(b)
LT = UT+8 hr
ICN (37.14°N, 127.54°E, Geom. 28.11°N)
(c)
LT = UT+9 hr
WU (30.5°N, 114.4°E,Geom. 21.04°N)
(d)
LT = UT+8 hr
SA (18.34°N, 109.42°E, Geom. 8.87°N)
(e)
LT = UT+8 hr
GUA (13.62°N, 144.86°E, Geom. 6.12°N)
(f)
LT = UT+9.6 hr
h'F (km)
UT (hours)

Figure 6 (a-e)

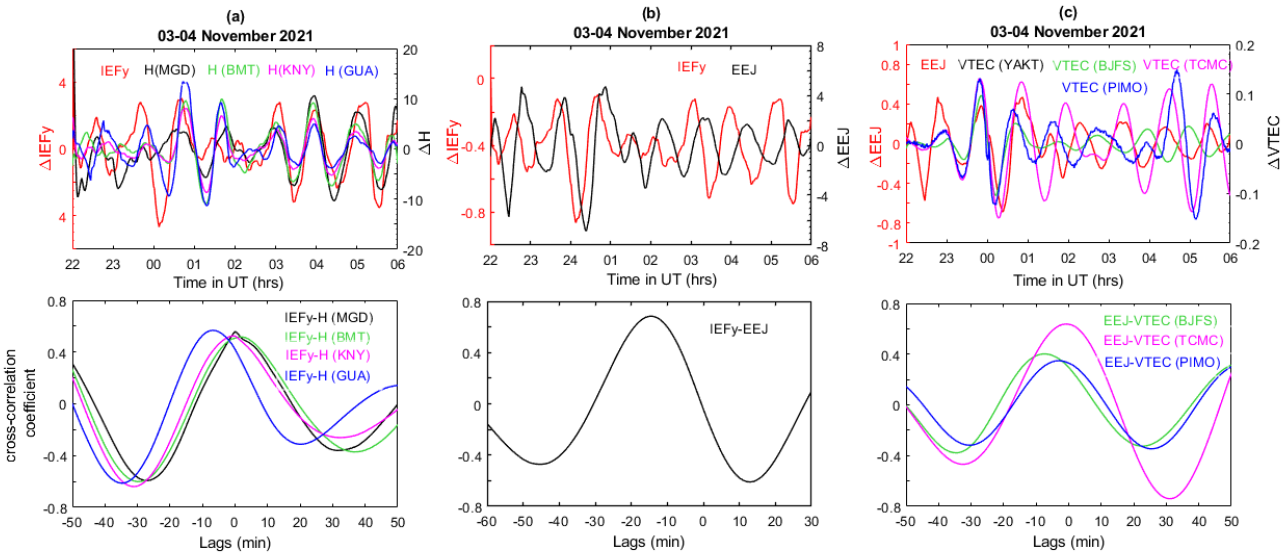
(a)
03-04 November 2021
IEFy
H(MGD)
H (BMT)
H(KNY)
H (GUA)
ΔIEFy
ΔH
Time in UT (hrs)
(b)
03-04 November 2021
IEFy
EEJ
ΔIEFy
ΔEEJ
Time in UT (hrs)
(c)
03-04 November 2021
EEJ
VTEC (YAKT)
VTEC (BJFS)
VTEC (TCMC)
VTEC (PIMO)
ΔEEJ
ΔVTEC
Time in UT (hrs)
cross-correlation coefficient
IEFy-H (MGD)
IEFy-H (BMT)
IEFy-H (KNY)
IEFy-H (GUA)
Lags (min)
IEFy-EEJ
Lags (min)
EEJ-VTEC (BJFS)
EEJ-VTEC (TCMC)
EEJ-VTEC (PIMO)
Lags (min)

Figure 7(a-c)

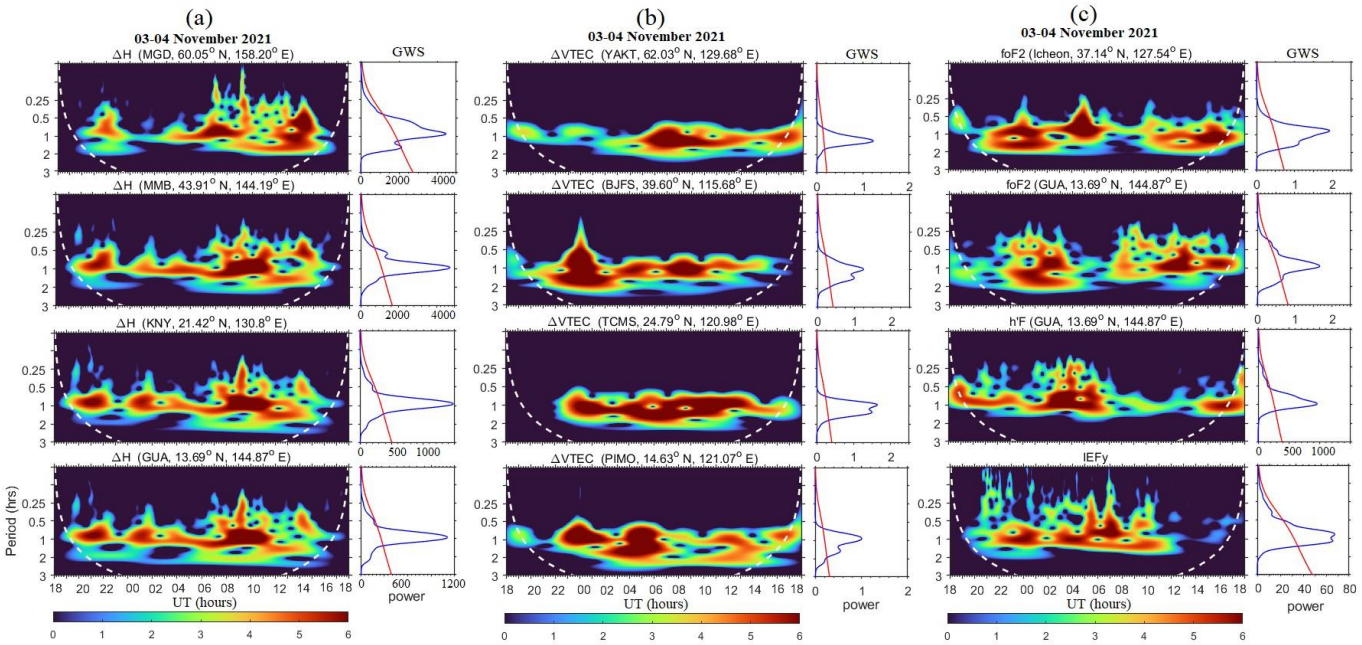
(a)
03-04 November 2021
ΔH (MGD, 60.05° N, 158.20° E)
ΔH (MMB, 43.91° N, 144.19° E)
ΔH (KNY, 21.42° N, 130.8° E)
ΔH (GUA, 13.69° N, 144.87° E)
GWS
(b)
03-04 November 2021
ΔVTEC (YAKT, 62.03° N, 129.68° E)
ΔVTEC (BJFS, 39.60° N, 115.68° E)
ΔVTEC (TCMS, 24.79° N, 120.98° E)
ΔVTEC (PIMO, 14.63° N, 121.07° E)
GWS
(c)
03-04 November 2021
foF2 (Icheon, 37.14° N, 127.54° E)
foF2 (GUA, 13.69° N, 144.87° E)
h'F (GUA, 13.69° N, 144.87° E)
IEFy
GWS
Period (hrs)
UT (hours)
power

Figure 8(a-c)